Check for updates

Quantification of defects engineered in single layer MoS$_2$†

Frederick Aryeetey,[a] Tetyana Ignatova [ID]*[b] and Shyam Aravamudhan [ID]*[a]

Atomic defects are controllably introduced in suspended single layer molybdenum disulfide (1L MoS$_2$) using helium ion beam. Vacancies exhibit one missing atom of molybdenum and a few atoms of sulfur. Quantification was done using a Scanning Transmission Electron Microscope (STEM) with an annular detector. Experimentally accessible inter-defect distance was employed to measure the degree of crystallinity in 1L MoS$_2$. A correlation between the appearance of an acoustic phonon mode in the Raman spectra and the inter-defect distance was established, which introduces a new methodology for quantifying defects in two-dimensional materials such as MoS$_2$.

Introduction

Monolayer molybdenum disulfide (1L MoS$_2$) belongs to the transition metal dichalcogenide (TMDC) family and is being extensively explored for applications in next-generation electronics. In general, all TMDC materials can be represented in form of MX$_2$ (M = Ti, Zr, Hf, V, Nb, Ta, Re, Mo, W; X = S, Se, Te), they are famous due to their ability to crystallize into layered two-dimensional (2D) structures.[1–5] In this case, the 2D MoS$_2$ crystal is made up of a molybdenum atomic layer sandwiched between two atomic layers of closely packed sulfur atoms. 1L MoS$_2$ has demonstrated several unique optical and optoelectronic properties for a wide range of applications.[2,6–10] Furthermore, 1L MoS$_2$, being a direct bandgap semiconductor, opens up the possibility for energy-efficient field effect transistors, photodetectors, solar cells and other optoelectronic devices. However, the practicability of realizing these applications hinges upon the synthesis of high quality, large area of MoS$_2$ monolayers. Large area and high-quality 1L MoS$_2$ can be made by using Chemical Vapor Deposition (CVD). Yet when compared to mechanical exfoliated samples, the CVD grown monolayers usually have lower carrier mobility due to inherent defects such as sulfur vacancies introduced during the growth process.[11,12] It has been reported that these structural defects in 1L MoS$_2$ can influence the mechanical, optical and electrical properties of the material[13] due to local modification of MoS$_2$ band structure in the vicinity of the defected spots.[14] Also, several approaches

have been reported in literature for creating and controlling density of sulfur vacancies by using electron or ion irradiation, thermal annealing and plasma treatment.[15–18] The development of these methods is crucial and intensely under investigation for controlling the material properties to match the requirements in different applications. It has been reported that Raman spectroscopy has emerged a powerful nondestructive characterization tool to quantify the defects controllably created in 1L MoS$_2$ by calculation the inter-defect distance (L_D).[19] The characteristic (E$_{2g}$, A$_{1g}$) peaks of the Raman active modes broaden with increasing defect density. This is accompanied by a downshift of the position of the E$_{2g}$ peak and an upshift of the position of the A$_{1g}$ peak.[20–23] With the increase in vacancy concentration, there are fewer Mo–S bonds involved in the in-plane vibration; therefore, the E$_{2g}$ peak is weakened and red shifted. The A$_{1g}$ peak corresponds to the out-of-plane vibration of Mo–S bonds with the Mo atom as a static center for 1L MoS$_2$. The restoring force constant is reduced because of missing Mo–S bond. Therefore, the originally static Mo atom is allowed to vibrate out-of-plane, which strengthens the restoring force constant from Mo–S vibration. This results in the blueshift of the A$_{1g}$ peak. Additionally, we expect appearance of the longitudinal acoustic mode peak at 227 cm^{-1} which is attributed to disorder-induced Raman scattering with momentum $q \neq 0$ at M point.

In this article, we report on using helium ion irradiation, to controllably introduce defects in 1L MoS$_2$ and then, we quantify the degree of crystallinity of 1L MoS$_2$ using Scanning Transmission Electron Microscope (STEM) and Raman spectroscopy. We have also investigated the correlation between ratio of Longitudinal Acoustic (LA) Raman active mode with respect to transverse optical A$_{1g}$ Raman mode and the experimentally accessible inter-defect distance from STEM analysis.

[a]Department of Nanoengineering, North Carolina A&T State University, 2907 East Gate City Blvd, Greensboro, North Carolina, 27401, USA. E-mail: saravamu@ncat.edu
[b]Department of Nanoscience, University of North Carolina at Greensboro, 2907 East Gate City Blvd, Greensboro, North Carolina, 27401, USA. E-mail: t_ignato@uncg.edu

† Electronic supplementary information (ESI) available: Details of wet transfer method, calculation of average of inter-defect distance in 1L MoS$_2$, additional Raman studies of irradiated MoS$_2$ on TEM grid and AFM measurements. See DOI: 10.1039/d0ra03372c

Experimental

The MoS_2 was grown on Si/SiO_2 substrate on a home-built chemical vapor deposition (CVD) system. Synthesis was optimized wherein molybdenum(vi) oxide and sulfur precursors react in vapor phase to deposit 1–2 layers of high quality MoS_2 monolayers (thickness $\sim$ 1 nm). Zeiss Orion Helium Ion Microscope (HeIM) was used to study the morphology and structure of MoS_2. Later, using HeIM's nanofabrication mode and operating at accelerating voltage of 30 kV, MoS_2 samples were irradiated. The exposure was performed using HeIM's patterning software to raster focused helium ion beam over an area varying between 10–50 μm by 10–50 μm in all single layer MoS_2. A blanker current of 5 pA was used for all doses and dwell time per pixel. The Raman spectra were collected at room temperature in ambient conditions on both pristine and irradiated samples using a Horiba XploRA Raman Confocal Microscope at 532 nm wavelength excitation, with 2400 L mm^{-1} grating. Atomic resolution images of 1L samples transferred onto Quantaifoil TEM grids were recorded using Nion Ultra HAADF-STEM operating at 60 kV with 3rd-generation C3/C5 aberration corrector and 0.5 nA current in atomic-size probe $\sim$1.0–1.1 angstrom.

Results

Fig. 1(a) shows a helium ion microscope image of the MoS_2 sample transferred onto TEM grid using wet transfer method (see ESI†). The triangular shaped crystal is mostly single crystalline with lateral dimensions up to tens of micrometers. The atomic structure of MoS_2 was studied using High angle atomic-resolution annular dark field (HAADF) imaging on the STEM. This technique is highly sensitive to variations in the atomic number of atoms in the sample; therefore, there is a significant contrast difference between molybdenum atoms of $Z = 42$ and sulfur atoms of $Z = 16$. The HAADF-STEM image shows alternating bright Mo and less bright S sites arranging in hexagonal rings in Fig. 1(b), 2(a and b). The Fourier transform of the HAADF-STEM image is presented in Fig. 1(c), with hexagonal

symmetry in the Brillouin zone. The point defects such as vacancies, which are particularly observed in CVD grown MoS_2 because of the growth process, can also be controllably engineered. In the STEM-HAADF image of pristine (unirradiated) sample, we can see only a few sulfur vacancies and an antisite defect, which represent vacancy complex of Mo and nearby three sulfur (MoS_3) atoms. This may be due to the Mo rich environment in the growth process. We can identify antisite defects and sulfur vacancies at the lattice sites using atom-by-atom chemical analysis on the STEM-HAADF. The calculated defect density (from sulfur vacancies) in the pristine MoS_2 monolayer transferred onto TEM grid was found to be 2.8 × 10^{13} cm^{-2}, which agrees well with previously reported results.[1] The only regions in close proximity to the edges of the MoS_2 sample were significantly damaged due to imperfections in the transfer process.

Morphology and STEM-HAAF atomic structure of 1L MoS_2

Helium ion irradiated regions on the suspended samples were identified and imaged using STEM-HAADF technique. Fig. 3 shows HAADF images of MoS_2 after varying helium ion irradiation doses, namely 1×10^{14}, 3×10^{14}, 3.75×10^{14}, 4×10^{14}, 5×10^{14}, 1×10^{15}, 5×10^{15}, 1×10^{16}, and 1×10^{17} ions per cm^2. The HAADF intensity allows us to distinguish elements (such as Mo and S) and the atomic structure of defects. The generated defects are consistent with the sputtering rate of helium ion beam. To assess the effect of helium ion on the metal/sulfur atomic vacancies, the experimental average inter-defect distance between two defect spots were calculated from the STEM images. The L_D value was calculated manually from STEM image maps, as shown in Fig. 1S (in ESI†) for a representative dose of 10^{14} ions per cm^2. The L_D values with corresponding standard deviations for all doses are presented in Table 1. The results reveal that the degree of crystallinity of 1L MoS_2 decreases as the dose increases. The predominant defects present were single molybdenum-based vacancies (1Mo + yS) while the number of missing sulfur atoms differed. Fig. 2(a) and (b) shows the smallest defect that can controllably resolved and created respectively. With increasing He$^+$ ion dose, the number
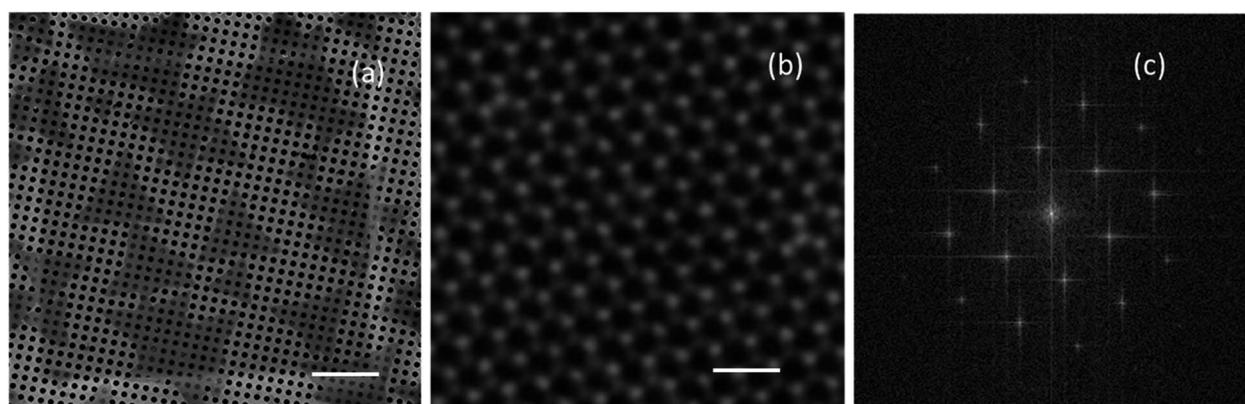

Fig. 1 (a) Helium ion image of 1L MoS_2 samples transferred onto TEM grid (scale bar is 2 μm). (b) Atomic-resolution STEM–HAADF image of pristine monolayer MoS_2, bright sites are molybdenum atoms and less bright sites are sulfur atoms (scale bar is 2 nm). (c) Fourier transform of the atomic structure of pristine 1L MoS_2.
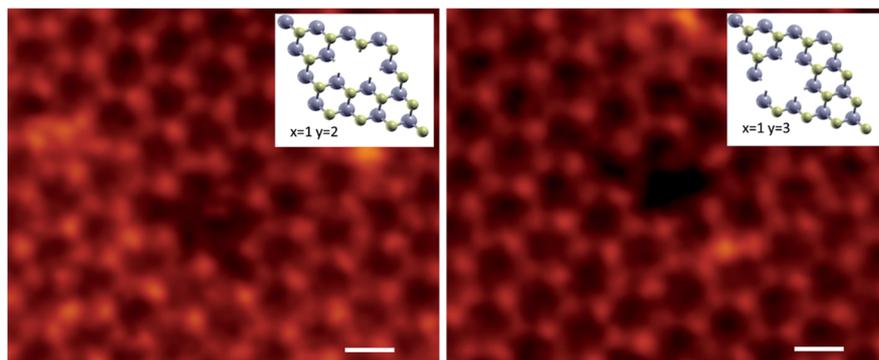
Fig. 2 High-magnification STEM images of atomic vacancies in different configurations (xMo + yS) showing single molybdenum-based vacancies at $x = 1$, while the number of missing sulfur atoms y varies: (a) $y = 2$; (b) $y = 3$. Scale bar is 0.3 nm.

of double sulfur based vacancies (1Mo + 2S) also increased and additionally triple sulfur based vacancies (1Mo + 3S) start to appear (Fig. 2(b)). Similar results were reported for Ga$^+$ ions at 10^{12} ions per cm^2.[24] It is important to note that the low mass of helium ions create gentle changes in crystallographic structure of 1L MoS$_2$ compared to results reported in literature with heavier ions.[25] At the highest dose of 1×10^{17} ions per cm^2, the MoS$_2$ crystal lattice is significantly distorted and damaged. The statistical analysis was performed using large area STEM images (Fig. 3) and plotted in Fig. 4(c).

Defect characterization of 1L MoS$_2$

Fourier transform of the STEM images following helium irradiation in the suspended MoS$_2$ samples reveals the crystallographic
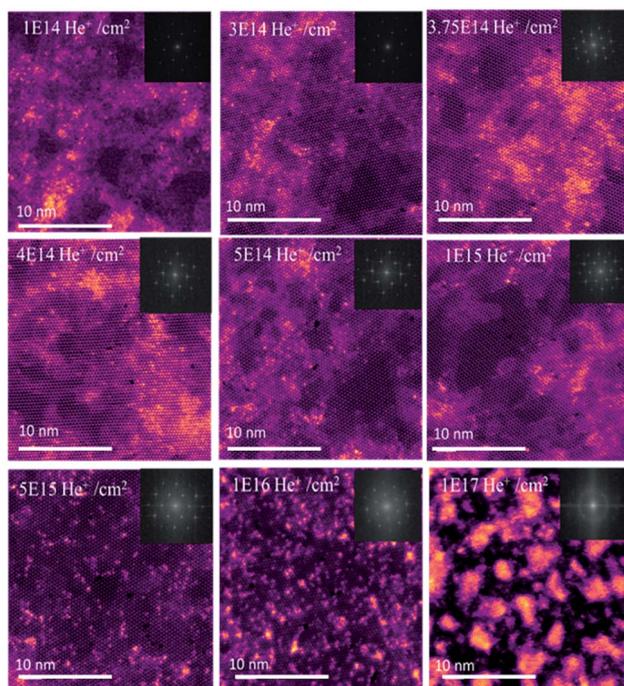

Fig. 3 Large STEM area characterization of defected 1L MoS$_2$ with different doses of irradiation from 1×10^{14} to 1×10^{17} He$^+$ per cm^2 used to calculate L_D, the FFT in insets show that sample is losing crystallinity completely at the dose 1×10^{17} He$^+$ per cm^2.

nature of MoS$_2$ (Fig. 3 insets). The broadening of diffraction spots with increase in dose from 1×10^{15} He$^+$ per cm^2 to 1×10^{17} He$^+$ per cm^2 is representation of breaking of the crystal symmetry and periodicity due to random scattering events and broadened Bragg diffraction.[26] The crystallinity of MoS$_2$ is intact for helium ion doses below 1×10^{15} ions per cm^2. Raman spectroscopy was additionally used to investigate the disorder effect in 1L MoS$_2$. For Raman characterization, we irradiated MoS$_2$ on Si substrate (the original growth substrate) with the same doses as used in the STEM-HAADF analysis. The results were identical to Raman characterization of suspended MoS$_2$ (see ESI†). Similar to the previously reported data,[20] (in-plane E$_{2g}$)/(out-of-plane A$_{1g}$) vibrational modes were red/blue shifted and both modes broadened after helium irradiation. In addition, a shoulder (at around 362 cm^{-1}) on the left of E$_{2g}$ peak and another one (around 415 cm^{-1}) to the right of A$_{1g}$ peak, which are assigned as defect modes in 1L MoS$_2$ were evident.[20,27,28] The evolution of Raman peaks for varying helium ion doses are presented in Fig. 4(a). Disorder-induced Raman scattering peaks appeared with the increase in dose from 10^{14} to 10^{16} He$^+$ per cm^2. In addition, a peak related to the MoS$_2$ longitudinal acoustic (LA) branch at the edge of the Brillouin zone, with the maximum at 227 cm^{-1} corresponding to the LA phonon at M point[20] also appeared. The LA modes were activated when defects were introduced into the MoS$_2$ lattice. Their relative intensities with

Table 1 The calculated value for the inter-defect distance from STEM imaging, ratio of Raman disorder, and the relation between STEM and Raman characterization

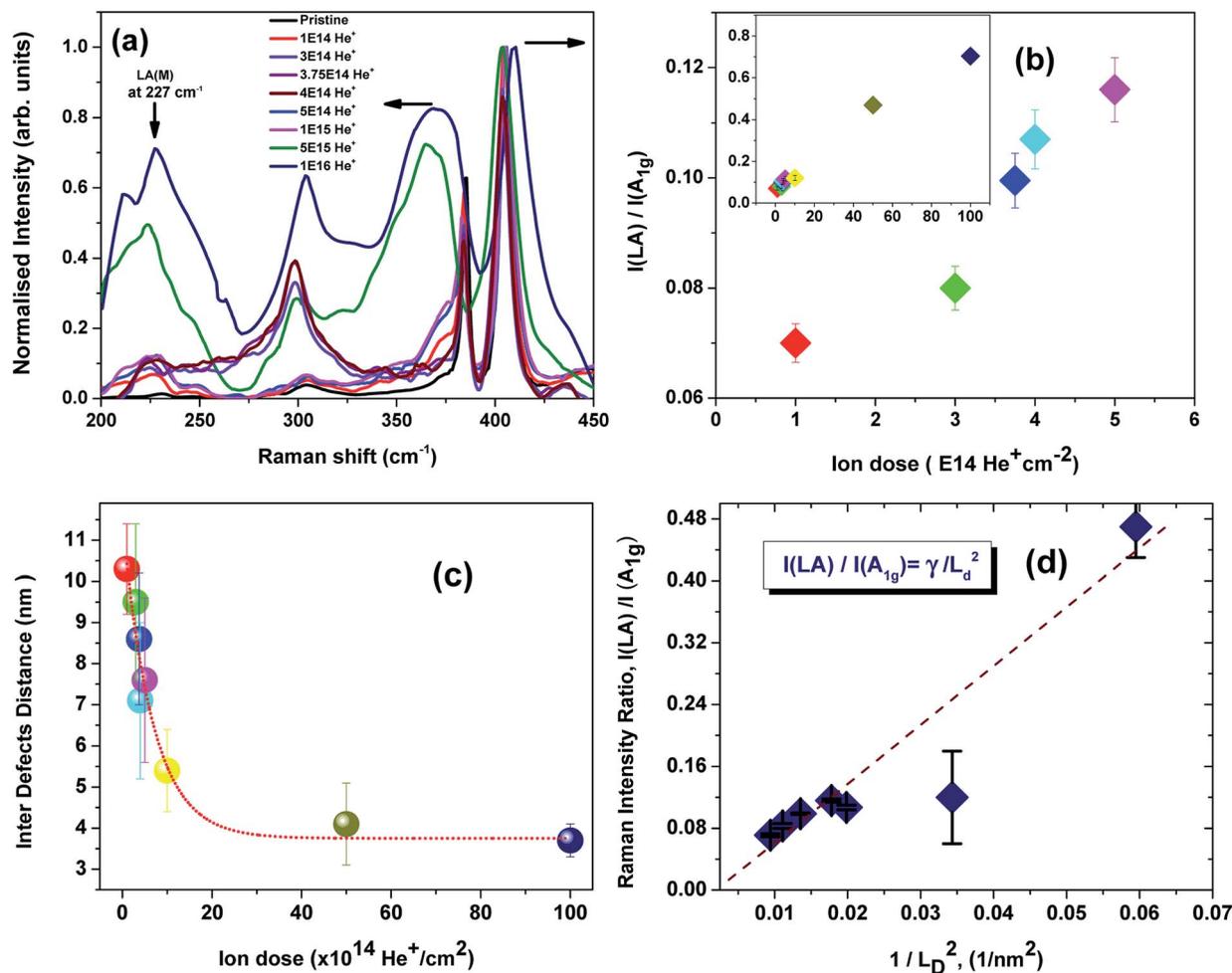| Helium ion dose (He$^+$ per cm^2)	L_D, nm (from STEM)	$\dfrac{I(\mathrm{LA})}{I(\mathrm{A_{1g}})}$	$\dfrac{\gamma}{L_D{}^2}$
1×10^{14}	10.3 ± 1.1	0.071	0.0701
3×10^{14}	9.5 ± 1.9	0.083	0.0831
3.75×10^{14}	8.6 ± 1.6	0.099	0.101
4×10^{14}	7.1 ± 1.9	0.107	0.148
5×10^{14}	7.5 ± 2.0	0.116	0.13
1×10^{15}	5.4 ± 1.0	0.120	0.257
5×10^{15}	4.1 ± 1.0	0.470	0.446
1×10^{16}	3.7 ± 0.4	0.704	0.547

Fig. 4 (a) Raman studies of irradiated 1L MoS_2 on silicon substrate; the first order Raman modes (E_{2g}/A_{1g}) are red/blue shifted and the second order mode LA(M) arises upon dosage increase; a peak at 300 cm^{-1} is related to Si acoustic mode; (b) ratio of intensity of longitudinal acoustic mode *versus* out of plane vibration mode of 1L MoS_2 for doses up to 5×10^{15} He^+ per cm^2, the whole range of doses *vs.* ratio presented in the inset; (c) plot of calculated inter defect distance *versus* helium ion dose from STEM characterization; (d) correlation between the inter-defect distance and Raman data for 1L MoS_2.

respect to the A_{1g} mode can be used as an indicator of the degree of crystallinity, as suggested previously in:[20]

$$\frac{I(\text{LA})}{I(A_{1g})} = \frac{\gamma}{L_D^2}, \tag{1}$$

where γ is the correlation constant and L_D is inter-defect distance (calculated from STEM analysis). The results of calculated ratio are plotted on Fig. 4(b). The dependency is linear with respect to He^+ ion doses up to a critical value of 5×10^{15} He^+ per cm^2. The data are in good agreement with the STEM-HAADF analysis of suspended MoS_2 monolayers, which also allows us to calculate the correlation constant $\gamma = 7.50$ nm^2. It is known that γ is dependent on the wavelength of excitation.[29–31] The calculation is based on excitation of 532 nm or 2.3 eV. A graph of the calculated L_D versus each helium ion doses is exhibits an exponentially decreasing function whose slope is equal to the slope of the normalized intensity ratio between longitudinal acoustic mode and out of vibration mode. Finally, the L_D and $I(\text{LA})/I(A_{1g})$ are related by eqn (1) using the table of

values (Table 1). Fig. 4(d) shows a straight-line dependency when intensity ratio is plotted *versus* inverse of the inter-defect distance with the slope equal to γ.

Conclusions

In this report, we presented an elegant and efficient method that can be used to quantify atomic vacancies with sulfur terminations in 1L MoS_2 created by helium ion irradiation. It is important to note that low mass of helium ion allows us to study gentle changes in crystallographic structure compared other data in literature using significantly heavier ions. For the first time, this paper reports on the generation and identification of (1Mo + 2S) defects. In addition, a combination of Raman and STEM measurements were used to calculate the correlation coefficient $\gamma = 7.50$ nm^2. Finally, the Raman characterization agrees well with STEM measurements on decreasing degree of crystallinity in 1L MoS_2 with increase in ion irradiation dose. In future, we plan to systematically study and compare the effect of

helium ion irradiation in mono and few-layers of MoS_2 using the above techniques in relation to conventional techniques such as XPS and XRD.

Conflicts of interest

There are no conflicts to declare.

Acknowledgements

Notes and references

1 M. Chhowalla, H. S. Shin, G. Eda, L. Li, K. P. Loh and H. Zhang, The chemistry of two-dimensional layered transition metal dichalcogenide nanosheets, *Nat. Chem.*, 2013, **5**(4), 263–275, DOI: 10.1038/nchem.1589.

2 Q. H. Wang, K. Kalantar-Zadeh, A. Kis, J. N. Coleman and M. S. Strano, Electronics and optoelectronics of two-dimensional transition metal dichalcogenides, *Nat. Nanotechnol.*, 2012, **7**(11), 699–712, DOI: 10.1038/nnano.2012.193.

3 R. Ganatra and Q. Zhang, Few-Layer MoS_2: A Promising Layered Semiconductor, *ACS Nano*, 2014, **8**(5), 4074–4099, DOI: 10.1021/nn405938z.

4 A. Splendiani, L. Sun, Y. Zhang, T. Li, J. Kim, C. Chim and F. Wang, Emerging Photoluminescence in Monolayer MoS_2, *Nano Lett.*, 2010, **10**(4), 1271–1275, DOI: 10.1021/nl903868w.

5 T. Verhagen, V. L. Guerra, G. Haider, M. Kalbac and J. Vejpravova, Towards the evaluation of defects in MoS_2 using cryogenic photoluminescence spectroscopy, *Nanoscale*, 2020, **12**, 3019–3028, DOI: 10.1039/C9NR07246B.

6 L. Gao, Q. Liao, X. Zhang, X. Liu, L. Gu, B. Liu and Z. Zhang, Defect-Engineered Atomically Thin MoS_2 Homogeneous Electronics for Logic Inverters, *Adv. Mater.*, 2020, **32**(2), 1906646, DOI: 10.1002/adma.201906646.

7 B. Radisavljevic, A. Radenovic, J. Brivio, V. Giacometti and A. Kis, Single-layer MoS_2 transistors, *Nat. Nanotechnol.*, 2011, **6**(3), 147–150, DOI: 10.1038/nnano.2010.279.

8 Z. Yin, H. Li, H. Li, L. Jiang, Y. Shi, Y. Sun and H. Zhang, Single-Layer MoS_2 Phototransistors, *ACS Nano*, 2011, **6**(1), 74–80, DOI: 10.1021/nn2024557.

9 Z. Zeng, Z. Yin, X. Huang, H. Li, Q. He, G. Lu and H. Zhang, Single-Layer Semiconducting Nanosheets: High-Yield Preparation and Device Fabrication, *Angew. Chem.*, 2011, **123**(47), 11289–11293, DOI: 10.1002/ange.201106004.

10 K. F. Mak, K. He, J. Shan and T. F. Heinz, Control of valley polarization in monolayer MoS_2 by optical helicity, *Nat. Nanotechnol.*, 2012, **7**(8), 494–498, DOI: 10.1038/nnano.2012.96.

11 Y. Lee, X. Zhang, W. Zhang, M. Chang, C. Lin, K. Chang and T. Lin, Synthesis of Large-Area MoS_2 Atomic Layers with Chemical Vapor Deposition, *Adv. Mater.*, 2012, **24**(17), 2320–2325, DOI: 10.1002/adma.201104798.

12 K. Liu, W. Zhang, Y. Lee, Y. Lin, M. Chang, C. Su and L. Li, Growth of Large-Area and Highly Crystalline MoS_2 Thin Layers on Insulating Substrates, *Nano Lett.*, 2012, **12**(3), 1538–1544, DOI: 10.1021/nl2043612.

13 F. Banhart, J. Kotakoski and A. V. Krasheninnikov, Structural Defects in Graphene, *ACS Nano*, 2010, **5**(1), 26–41, DOI: 10.1021/nn102598m.

14 D. Rhodes, S. H. Chae, R. Ribeiro-Palau and J. Hone, Disorder in van der Waals heterostructures of 2D materials, *Nat. Mater.*, 2019, **18**, 541–549, DOI: 10.1038/s41563-019-0366-8.

15 S. Bertolazzi, S. Bonacchi, G. Nan, A. Pershin, D. Beljonne and P. Samorì, Engineering Chemically Active Defects in Monolayer MoS_2 Transistors *via* Ion-Beam Irradiation and Their Healing *via* Vapor Deposition of Alkanethiols, *Adv. Mater.*, 2017, **29**(18), 1606760, DOI: 10.1002/adma.201606760.

16 A. V. Krasheninnikov and K. Nordlund, Ion and electron irradiation-induced effects in nanostructured materials, *J. Appl. Phys.*, 2010, **107**(7), 071301, DOI: 10.1063/1.3318261.

17 D. S. Fox, Y. Zhou, P. Maguire, A. O'Neill, C. Ó'Coileáin, R. Gatensby and H. Zhang, Nanopatterning and Electrical Tuning of MoS_2 Layers with a Subnanometer Helium Ion Beam, *Nano Lett.*, 2015, **15**(8), 5307–5313, DOI: 10.1021/acs.nanolett.5b01673.

18 D. Fox, Y. B. Zhou, A. O'Neill, S. Kumar, J. J. Wang, J. N. Coleman and H. Z. Zhang, Helium ion microscopy of graphene: beam damage, image quality and edge contrast, *Nanotechnology*, 2013, **24**(33), 335702, DOI: 10.1088/0957-4484/24/33/335702.

19 V. Iberi, L. Liang, A. V. Ievlev, M. G. Stanford, M. Lin, X. Li and O. S. Ovchinnikova, Nanoforging Single Layer $MoSe_2$ Through Defect Engineering with Focused Helium Ion Beams, *Sci. Rep.*, 2016, **6**(1), 1–9, DOI: 10.1038/srep30481.

20 S. Mignuzzi, A. J. Pollard, N. Bonini, B. Brennan, I. S. Gilmore, M. A. Pimenta and D. Roy, Effect of disorder on Raman scattering of single-layer MoS_2, *Phys. Rev. B: Condens. Matter Mater. Phys.*, 2015, **91**(19), 195411, DOI: 10.1103/physrevb.91.195411.

21 A. J. Pollard, B. Brennan, H. Stec, B. J. Tyler, M. P. Seah, I. S. Gilmore and D. Roy, Quantitative characterization of defect size in graphene using Raman spectroscopy, *Appl. Phys. Lett.*, 2014, **105**(25), 253107, DOI: 10.1063/1.4905128.

22 V. Carozo, C. M. Almeida, E. H. Ferreira, L. G. Cançado, C. A. Achete and A. Jorio, Raman Signature of Graphene

Superlattices, *Nano Lett.*, 2011, **11**(11), 4527–4534, DOI: 10.1021/nl201370m.

23 E. H. Martins Ferreira, M. V. Moutinho, F. Stavale, M. M. Lucchese, R. B. Capaz, C. A. Achete and A. Jorio, Evolution of the Raman spectra from single-, few-, and many-layer graphene with increasing disorder, *Phys. Rev. B: Condens. Matter Mater. Phys.*, 2010, **82**(12), 125429, DOI: 10.1103/physrevb.82.125429.

24 J. P. Thiruraman, K. Fujisawa, G. Danda, P. M. Das, T. Zhang, A. Bolotsky, N. Perea-López, A. Nicolaï, P. Senet, M. Terrones and M. Drndić, Angstrom-Size Defect Creation and Ionic Transport through Pores in Single-Layer MoS_2, *Nano Lett.*, 2018, **18**(3), 1651–1659, DOI: 10.1021/acs.nanolett.7b04526.

25 J. Hong, Z. Hu, M. Probert, K. Li, D. Lv, X. Yang and Z. Zhang, Exploring atomic defects in molybdenum disulphide monolayers, *Nat. Commun.*, 2015, **6**(1), 1–8, DOI: 10.1038/ncomms7293.

26 M. G. Stanford, P. R. Pudasaini, A. Belianinov, N. Cross, J. H. Noh, M. R. Koehler and P. D. Rack, Focused helium-ion beam irradiation effects on electrical transport properties of ew-layer WSe_2: enabling nanoscale direct write homo-junctions, *Sci. Rep.*, 2016, **6**(1), 27276, DOI: 10.1038/srep27276.

27 G. L. Frey, R. Tenne, M. J. Matthews, M. S. Dresselhaus and G. Dresselhaus, Optical Properties of MS_2 (M = Mo, W) Inorganic Fullerenelike and Nanotube Material Optical Absorption and Resonance Raman Measurements, *J. Mater. Res.*, 1998, **13**(9), 2412–2417, DOI: 10.1557/jmr.1998.0335.

28 Y. Chen, S. Huang, X. Ji, K. Adepalli, K. Yin, X. Ling and B. Yildiz, Tuning Electronic Structure of Single Layer MoS_2 through Defect and Interface Engineering, *ACS Nano*, 2018, **12**(3), 2569–2579, DOI: 10.1021/acsnano.7b08418.

29 F. Tuinstra and J. L. Koenig, Raman Spectrum of Graphite, *J. Chem. Phys.*, 1970, **53**(3), 1126–1130, DOI: 10.1063/1.1674108.

30 L. G. Cançado, A. Jorio, E. H. Ferreira, F. Stavale, C. A. Achete, R. B. Capaz and A. C. Ferrari, Quantifying Defects in Graphene *via* Raman Spectroscopy at Different Excitation Energies, *Nano Lett.*, 2011, **11**(8), 3190–3196, DOI: 10.1021/nl201432g.

31 P. Venezuela, M. Lazzeri and F. Mauri, Theory of double-resonant Raman spectra in graphene: intensity and line shape of defect-induced and two-phonon bands, *Phys. Rev. B*, 2011, **84**(3), 035433, DOI: 10.1103/physrevb.84.035433.